ACS OMEGA

Open Access

http://pubs.acs.org/journal/acsodf

Article

Synthesis and Characterization of Durable Antibiofilm and Antiviral Silane-Phosphonium Thin Coatings for Medical and Agricultural Applications

Matan Nissim, Taly lline-Vul, Sivan Shoshani, Gila Jacobi, Eyal Malka, Aviv Dombrovsky, Ehud Banin, and Shlomo Margel*

Cite This: *ACS Omega* 2023, 8, 39354−39365

Read Online

ACCESS | Metrics & More | Article Recommendations

ABSTRACT: Pathogens such as bacteria and viruses cause disease in a range of hosts, from humans to plants. Bacterial biofilms, communities of bacteria, e.g., *Staphylococcus aureus*and *Escherichia coli*, attached to the surface, create a protective layer that enhances their survival in harsh environments and resistance to antibiotics and the host's immune system. Biofilms are commonly associated with food spoilage and chronic infections, posing challenges for treatment and prevention. Tomato brown rugose fruit virus (ToBRFV), a newly discovered tobamovirus, infects tomato plants, causing unique symptoms on the fruit, posing a risk for tomato production. The present study focuses on the effectiveness of silane-phosphonium thin coatings on polymeric films, e.g., polypropylene. Phosphonium has significant antibacterial activity and is less susceptible to antibacterial resistance, making it a safer alternative with a reduced environmental impact. We successfully synthesized silane-phosphonium monomers as confirmed by ^{31}P NMR and mass spectrometry. The chemical composition, thickness, morphology, and wetting properties of the coatings were tested by Fourier-transform infrared spectroscopy with attenuated total reflectance, focused ion beam, atomic force microscopy, environmental scanning electron microscope, and contact angle (CA) measurements. The antibiofilm and antibacterial activities of the coatings were tested against *S. aureus* and *E. coli*, while the antiviral activity was evaluated against ToBRFV. The significant antibiofilm and antiviral activity suggests applications in various fields including medicine, agriculture, and the food industry.

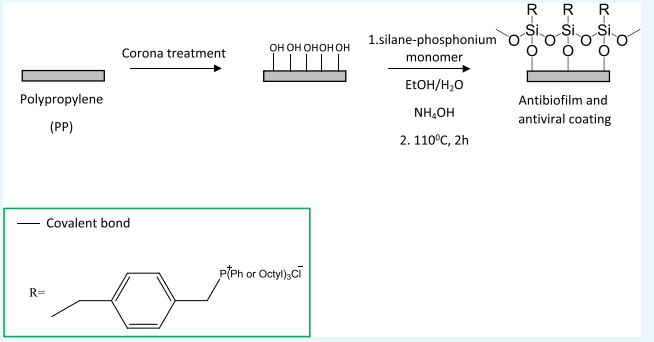

1. INTRODUCTION

Pathogens, such as bacteria or viruses, are microorganisms capable of causing disease in animals, plants, and humans.[1,2] Bacterial biofilms are communities of bacteria that attach to surfaces and to each other by a self-produced matrix. The biofilm mode of growth provides bacteria with increased resilience to extreme environments, antibiotics, and immune systems.[2,3] Biofilms play a crucial role in many aspects of daily life including food spoilage and hospital acquired infections.[4−10]

Similarly, viruses can also cause disease and food spoilage.[11−13] The tomato brown rugose fruit virus (ToBRFV) is a newly discovered plant virus that belongs to the tobamovirus family and can cause disease in tomatoes[14] and pepper varieties lacking *L* resistant alleles.[15] Since its discovery in Jordan and Israel in 2014 and 2015,[14,16] respectively, ToBRFV spread to other countries, including Germany, the United States, Turkey, and China.[11,12]

ToBRFV causes significant economic damage to the tomato crops, which are one of the important crops grown worldwide.[11,13] The tobacco plant *Nicotiana glutinosa*produces a hypersensitive response (HR) when infected with ToBRFV,[13] resulting in necrotic local lesions (LLs) that isolate the virus and prevent it from spreading throughout the plant.

Many studies focus on the development of biocides and the prevention of infection.[17,18] However, these biocides can lead to antimicrobial resistance and environmental pollution and can be toxic to humans.[17]

Phosphonium salts, which are positively charged, exhibit potent antibacterial activity against a wide range of microorganisms.[17−22] These salts are absorbed into the cytoplasmic

Received: July 9, 2023
Accepted: September 22, 2023
Published: October 12, 2023

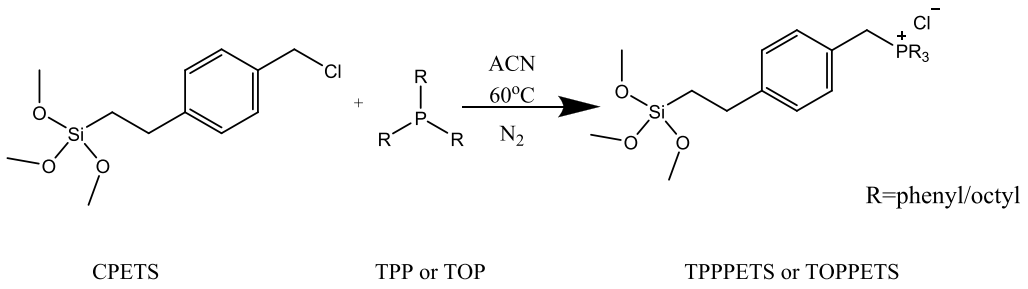

Figure 1. Synthesis of the silane-phosphonium monomers.

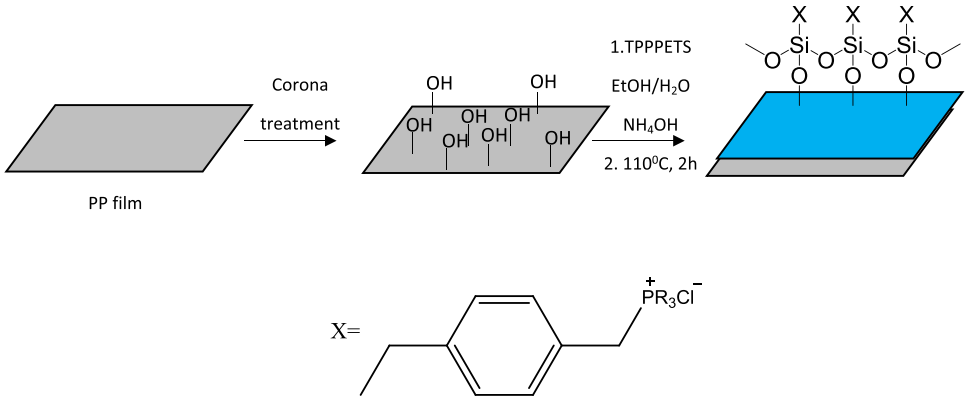

Figure 2. Coating process of PP films with phosphonium monomers. R = phenyl/octyl.

membrane, creating a disruption that leads to microbial cell death.[17−19] In comparison to existing cationic disinfectants containing positively charged nitrogen atoms, phosphonium salts have significantly higher antimicrobial activity.[18,19] They are particularly effective against drug-resistant bacteria, such as methicillin-resistant *S. aureus*.[18] Furthermore, since these disinfectants target the bacterial cytoplasmic membrane, they are less susceptible to antibacterial resistance.[17,19−22] Our study focuses on the utilization of silane-phosphonium thin coatings onto polymeric films for medical, agricultural, and industrial purposes. The aims of these coatings are to inhibit bacterial biofilm formation while reducing the possibility of antibiotic resistance and development and providing an effective and stable antibiofilm and antiviral agent.

In this study, silane-phosphonium monomers were synthesized and used to coat a corona-discharged polypropylene (PP) surface. Corona-treatment is a method used to increase the surface energy, adhesion properties, surface wetting, polarity, and roughness of surfaces through an oxidation mechanism, which generates surface polar groups.[23−33] These polar groups, such as hydroxyl groups, can be used for chemical reactions, including the binding of silanol compounds. The coating was applied using the Mayer−Rod method, which is a well-known technique for creating thin, uniform films on different substrate surfaces through the even spreading of a liquid.[34−36] This coating method requires no special physical conditions. The materials and the fast-coating technique are simple, cost-effective, and can be used to coat different types of polymeric films.[34,35]

The present study demonstrated that the phosphonium-based coatings applied to the PP surface were highly effective in preventing the formation of *S. aureus*and *E. coli*biofilms. Furthermore, the coatings exhibited significant antiviral activity against ToBRFV. Moreover, the coatings onto the PP surface were found to be durable and long lasting.

These findings suggest that phosphonium-based coatings have great potential for use in various medical, agricultural, and industrial applications.

2. MATERIALS AND METHODS

2.1. Materials. The following high-purity chemicals were procured from various commercial suppliers: triphenylphosphine (TPP), trioctylphosphine (TOP), anhydrous acetonitrile (ACN), tetra orthosilicate (TEOS), and ammonium hydroxide aqueous solution (28%) were sourced from Sigma-Aldrich (Israel); ((chloromethyl)phenylethyl)trimethoxysilane (CPETS) was acquired from Gelest; anhydrous ethanol was obtained from Carlo Erba Reagents, Romical, Ltd. (Israel). Mapal Plastics generously provided PP films.

2.2. Methods. *2.2.1. Synthesis of Silane-Phosphonium Monomers.* In a dry flask under a N_2 atmosphere, TPP (1.00 g, 262.091 g/mol) or TOP (1.69 mL, 370.372 g/mol) was dissolved in dry ACN. The flask was dried overnight at 150 °C in an oven before use. Next, 960 μL of CPETS (274.079 g/mol) were added to the ACN solution, and the solution was heated to 60 °C for 24 h. Following this, the ACN was evaporated, resulting in the desired product being obtained.

Figure 1 shows the synthesis of the two monomers triphenyl/trioctyl(phosphoniummethyl)phenylethyl-trimethoxysilane chloride (TPPPETS/TOPPETS).

2.2.2. Thin coatings of SiO_2 and/or Poly(silane-phosphonium) onto Corona-Treated PP Films. PP films underwent corona discharge treatment (350 W·min/m^2). SiO_2-phosphonium thin coatings onto corona-treated PP films were prepared in two ways: (1) a modified Stöber polymerization[37−40] of the silane-phosphonium monomers TPPPETS/TOPPETS in ethanol/water continuous phase, followed by spreading the formed dispersion onto corona-treated PP films via Mayer Rod coating (bar no. 1, RK print coat instruments, U.K.); (2) a

https://doi.org/10.1021/acsomega.3c04908
ACS Omega 2023, 8, 39354−39365

Table 1. Composition of the Materials Used for Preparation of Phosphonium-Based Coatings[a]

coating type	water (mL)	ethanol (mL)	NH_4OH (mL)	TEOS (mL)	silane-phosphonium monomer (g)
SiO_2	2.652	7.5	0.18	0.2	
poly(TPPPETS)	7.5	2.652	0.18		TPPPETS (0.2)
SiO_2/poly(TPPPETS)	2.652	7.5	0.18	0.1	TPPPETS (0.1)
SiO_2/poly(TOPPETS)	2.652	7.5	0.18	0.1	TOPPETS (0.1)

[a]The coating made from poly(TOPPETS) was not at all uniform. Hence, the characterization and biological activities of this coating are not shown.

modified Stöber polymerization of TPPPETS/TOPPETS onto SiO_2 core NPs, followed by spreading via a Mayer Rod of the formed SiO_2/poly(silane-phosphonium) dispersion onto corona-treated PP films. Both coating processes were performed immediately after the solvation of the silane-phosphonium monomer.

In the second method, TEOS Stöber polymerization was done for 30 min. At this point, SiO_2 nanoparticles (NPs) begin to form so that there are many OH groups that replace methoxy groups in TEOS (produced by Stöber polymerization). These groups can react with other OH groups of TPPPETS/TOPPETS that are produced when adding these monomers and/or with OH groups of the corona-treated PP (water molecule released). TEOS has four link sites (four methoxy groups) unlike the silane-phosphonium monomer, which has only three link sites. Hence, the combination of silane-phosphonium monomer with TEOS after Stöber polymerization for a short time can improve the bonding of the silane-phosphonium monomer to the corona-treated PP. Therefore, the role of the TEOS is to connect the corona-treated PP film and the silane-phosphonium monomer coating by binding to both (after the methoxy group is replaced by a hydroxyl group).

As controls, pure PP, corona-treated PP, and PP with a SiO_2 coating were tested. All coatings were made with a size 1 Mayer Rod bar. Figure 2 shows the process for coating corona-treated PP films, and Table 1 shows the content of the materials used to create thin SiO_2-phosphonium coatings.

2.3. Characterizations. *2.3.1. ^{31}P Nuclear Magnetic Resonance (NMR) of the Silane-Phosphonium Monomers.* A powerful tool for examining the products is ^{31}P NMR. There is just one phosphine atom in each reactant (from TPP/TOP), and the synthetic method relies upon this nucleophile acting phosphine. As a result, the chemical shift of this phosphine changes significantly. All NMR spectra were acquired on samples dissolved in chloroform-D ($CDCl_3$, Cambridge Isotope Laboratories, USA) by using a Bruker DMX-400 spectrometer (161.9 MHz, Germany).

2.3.2. Mass Spectra (MS) of the Silane-Phosphonium Monomers. In addition to ^{31}P NMR, MS can show that silane-phosphonium monomers were synthesized. To confirm the molar mass of the positive ions in our products, high-resolution mass spectrometry (Q-TOF 6545 LC-MS (ESI/APCI/ASAP), Agilent, USA) was applied to validate the molar mass of the positive ion.

2.3.3. Characterization of the Chemical Composition of the Film Surfaces by FTIR/ATR. FTIR spectra for the different films were obtained at room temperature using the Bruker ALPHA-FTIR Quicksnap sampling module equipped with a platinum ATR diamond module (Bruker). The OPUS program was used to process and analyze the obtained data. The measurements were conducted in the range of 400−3000 cm^{-1}.

2.3.4. Determination of Coating Thickness by FIB. The coating thickness was determined by FIB (Helios 5 UC, Thermo Scientific, USA), using a cross section of the sample. Dry coated corona-treated PP films were attached to a silicon wafer with carbon tape and coated with iridium prior to FIB examination.

2.3.5. Determination of Film Surface Morphology and Roughness by AFM. The surfaces (roughness and morphology) of the films are different because of the various treatments done on each film. AFM measurements were conducted by using a Bio FastScan scanning probe microscope (Bruker AXS). The PeakForce quantitative nanomechanical mapping (QNM) mode was used with a FastScan-C silicon probe (Bruker) with a spring constant of 0.45 N/m. All measurements were carried out in an acoustic hood under controlled environmental conditions to minimize vibrational noise. The images were acquired in the retrace direction at a scan rate of 1.7 Hz with a resolution of 512 samples/line. Image processing and roughness analysis were done using Nanoscope Analysis software applying both "flatting" and "planefit" functions.

2.3.6. Characterization the Surfaces of the Coatings by ESEM and Determination of Phosphorus Percentage by EDX. In addition to FIB and AFM, ESEM can provide additional information about the uniformity and morphology of the coatings in larger scale than AFM. Hence, ESEM images were taken in small and large scales using an FEI E-SEM Quanta 200 F scanning electron microscope (Oregon, USA) operating at 15 kV (EDX operating at 5 kV). Dry coated corona-treated PP films were attached to a silicon wafer with carbon tape and coated with gold prior to ESEM imagination.

2.3.7. Wettability Properties by Contact Angle (CA) Measurements of the Films. Water CA measurements were performed by using a Goniometer (System OCA, model OCA20, Data Physics Instruments Gmbh, Filderstadt, Germany). Double distilled water drops (3 μL) were gently deposited on the surface by a syringe, and after the needle was removed from the drop, an image was taken.

2.3.8. Coating Durability. Examination of the coatings' stability was done by an adhesion test. An adhesive tape was attached to the coated films, and the film was peeled off. The process was done ten times for each coating, and at the end of the process, the CA of each coating was measured.

2.4. Biological Testing Methods. *2.4.1. Antibiofilm Activity.* Poly(TPPPETS), SiO_2/poly(TPPPETS) and SiO_2/poly(TOPPETS) coated surfaces were examined for antibiofilm and antibacterial activity, along with controls (PP, corona-treated PP, and SiO_2 coating surfaces). The coated surfaces were tested against one Gram-positive strain and one Gram-negative strain (*S. aureus*ATCC 29213 and *E. coli*ATCC 25922, respectively). The surfaces were precut into 1 cm^2 squares. For each experiment, the bacteria were grown overnight at 37 °C with continuous shaking at 250 rpm in 100% Mueller Hinton medium (MH, BD). To create bacterial

https://doi.org/10.1021/acsomega.3c04908
ACS Omega 2023, 8, 39354−39365

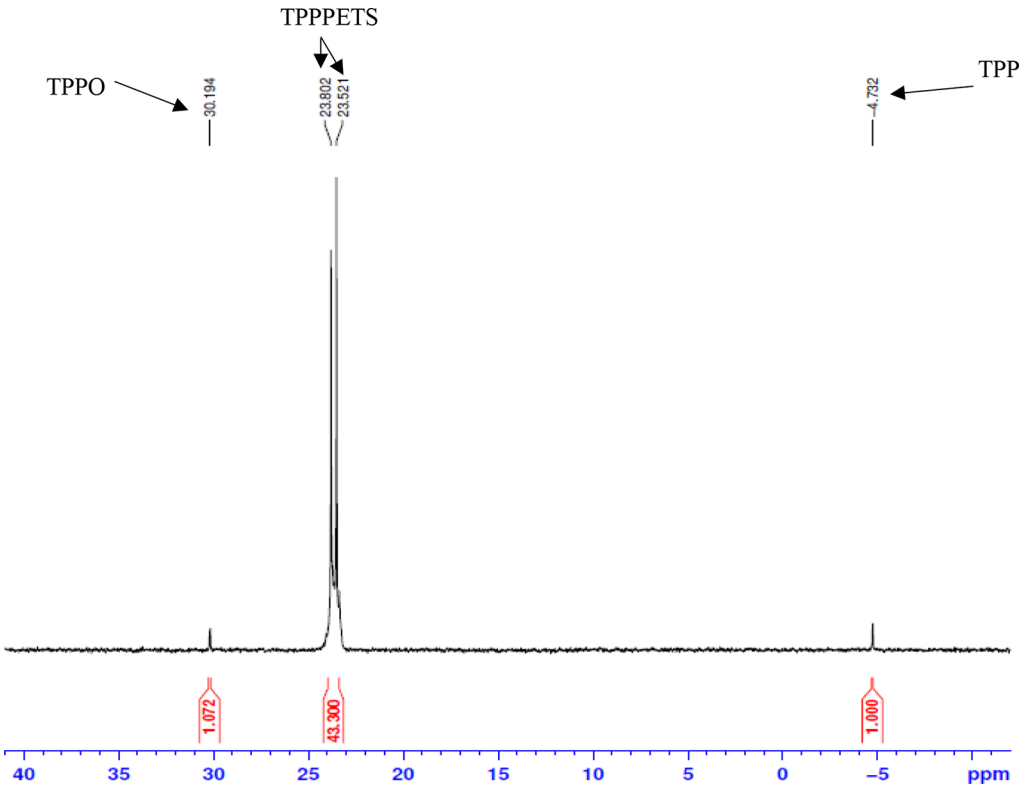

Figure 3. ^{31}P NMR spectrum of the as-prepared TPPPETS.

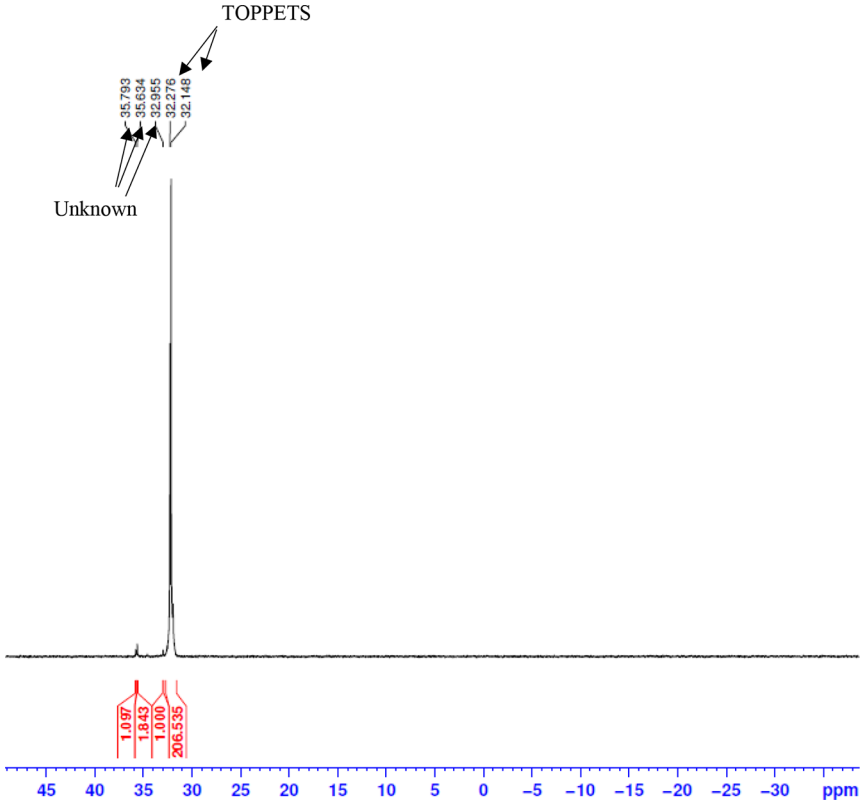

Figure 4. ^{31}P NMR spectra of as-prepared TOPPETS.

stocks, one percent MH was used to adjust the bacteria concentration to 0.01 O.D. for *S. aureus*and 0.3 O.D. for *E. coli*. Additionally, 0.2% glucose was added to the *S. aureus*stock. Next, the squares were glued to the bottom of a 24-well plate, and 1 mL of bacterial stock was transferred onto the glued squares. For *E. coli*, 1 mL of the stock was first dispensed into to each well of a 24-well plate, and subsequently, the squares were positioned on top of the liquid. In all experiments, the

https://doi.org/10.1021/acsomega.3c04908
ACS Omega 2023, 8, 39354−39365

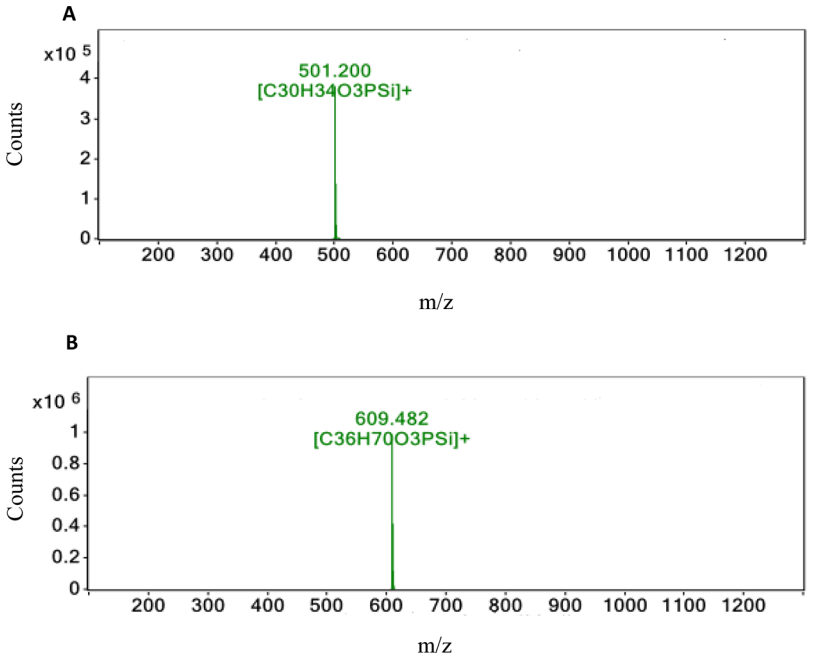

Figure 5. Mass spectrometry of the silane-phosphonium monomer: (A) TPPPETS and (B) TOPPETS.

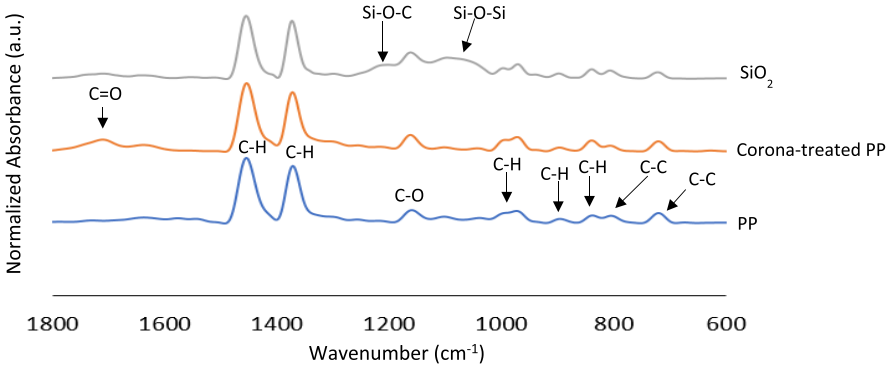

Figure 6. FTIR spectra of SiO_2 coating and pristine and corona-treated PP films.

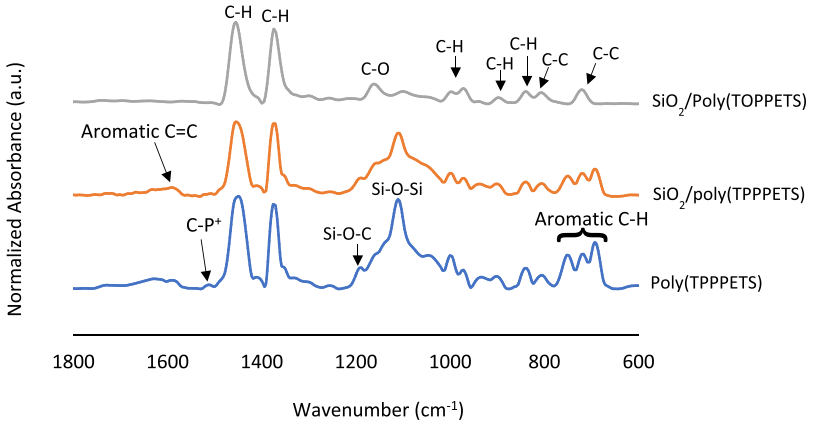

Figure 7. FTIR spectra of poly(TPPPETS), SiO_2/poly(TPPPETS) and SiO_2/poly(TOPPETS) coatings.

plates were incubated at 37 °C for approximately 18 h. Following incubation, two samples from the liquid phase were used to determine the quantity of the planktonic bacteria by the viable count method. For biofilm quantification, the squares were rinsed three times using sterile DDW, followed by scraping the biofilm into 250ul of medium. This suspension was used to quantify the bacteria within the biofilm by a viable count. The experiments were performed three times with two internal repeats.

2.4.2. Bioassay with Tomato Brown Rugose Fruit Virus (ToBRFV). For evaluation of the antiviral activity of the coatings, all prepared coatings were divided into two halves.

https://doi.org/10.1021/acsomega.3c04908
ACS Omega 2023, 8, 39354−39365

Only on one-half was a 1:5000 dilution of ToBRFV solution sprayed, and the two halves were attached for 24 h. Afterward, 0.2 mL of phosphate buffer was added to each half for extracting the remaining virus and viral particles. Leaves of the tobacco plant *N. glutinosa*were sprayed with silicon carbide (Carborundum) and exposed to the collected liquid. The appearance of LLs occurred 4 days post viral infection. Each test was performed on three leaves of three plants for a total of nine leaves, and LLs were counted. An LL reduction indicates a reduced viral load due to the decontamination effects of the coating sample. As a positive control, *N. glutinosa*leaves were sprayed with carborundum dust and exposed directly to 1:5000 dilutions of ToBRFV solution with 0.2 mL of phosphate buffer.

2.4.3. ELISA Detection of ToBRFV in Leaves of Tomato Plants. ELISA was used to identify the presence of ToBRFV infection in tomato plants, as the appearance of the infection was not easily distinguishable.[41] Tested leaves were collected from tomato plants that were infected with ToBRFV for 2 weeks. Indirect ELISAs (Thermo Fisher Multiskan FC) were performed on leaves that had ToBRFV infection symptoms. Samples were placed in a coating buffer (Agdia) and incubated for 3 h at 37 °C with a 1:5000 dilution of the ToBRFV antiserum. Detection was done by incubating the samples with AP-conjugated goat antirabbit IgG (Sigma, Germany) for 3 h at 37 °C. A substrate of *P*-nitro phenyl phosphate (Sigma) was used at a concentration of 0.6 mg/mL. The accepted color reaction was detected and recorded with an ELISA reader (Thermo Fisher Multiskan FC) at 405 and 620 nm. The minimum ratio OD values considered positive were determined to be three times higher than the value of the healthy (negative) controls.

3. RESULTS AND DISCUSSION

3.1. Characterization. *3.1.1. ^{31}P NMR of the Silane-Phosphonium Monomers.* One method for identifying phosphorus-containing products and determining their purity level is ^{31}P NMR analysis. This technique is particularly suitable for our desired products, which contain only one phosphorus atom, and is a straightforward approach. In the case of TPPPETS, the peaks indicating the presence of phosphonium are at 23.521 and 23.802 ppm, as shown in Figure 3. The two peaks result from a mixture of meta and para CPETS. The peak at −4.732 ppm corresponds to the unreacted phosphine atom of TPP, while another peak at 30.194 ppm is triphenylphosphine oxide (TPPO), which is probably produced as a byproduct during the synthesis of the silane-phosphonium monomer. Through integration, phosphonium was determined as the main product with a purity level of over 95%.

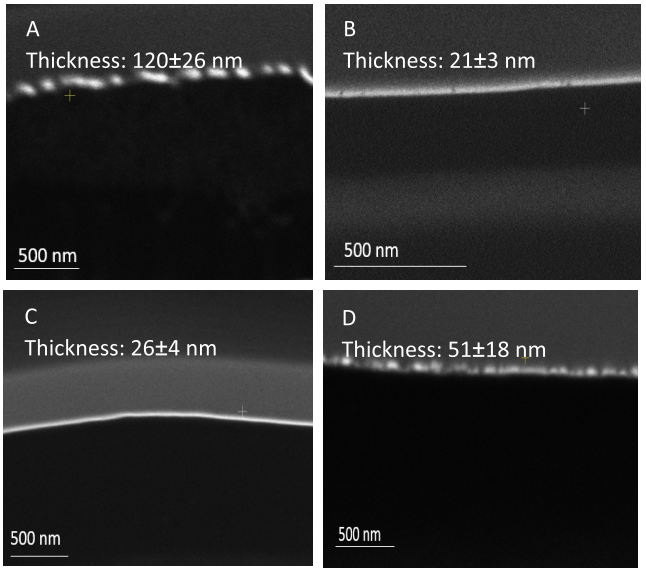

Figure 8. Thickness of the coatings studied by FIB. (A) SiO_2, (B) poly(TPPPETS), (C) SiO_2/poly(TPPPETS), and (D) SiO_2/poly-(TOPPETS).

Figure 4 shows TOPPETS, the chemical shifts of the phosphonium at 32.148 and 32.276 ppm, indicating a successful synthesis of TOPPETS with a purity level of over 95%. While some unknown impurities were detected, their integration shows that they had a negligible presence. Additionally, the lack of a phosphine peak for TOP, which typically appears around −30 ppm, indicates that there is no unreacted TOP present in the sample, suggesting a complete reaction between the phosphine source and TOP.

3.1.2. MS of the Silane-Phosphonium Monomers. The exact molar masses of TPPPETS and TOPPETS are 536.170 and 644.452 g/mol, respectively. By subtracting the negative ion of the monomer (chlorine ion), we can determine the exact mass of the positive ion can be determined. Figure 5 displays various masses resulting from different isotopes. These results provide evidence of the desired products.

3.1.3. Chemical Composition of the Film Surfaces. FTIR can be used to study functional groups present on the surfaces of the different films. Figure 6 displays FTIR measurements of pristine, corona-treated PP, and corona-treated PP coated with SiO_2. Significant differences between the substrates can be observed, including a peak at 1710 cm^{-1}, indicating a carbonyl stretching band resulting from corona treatment that is not found on the other surfaces. Additionally, a peak at 1040−1200 cm^{-1} corresponds to the Si−O−Si stretching band, which is only found in the SiO_2 coating. This is due to the high number of Si−O bonds present in the SiO_2 coating, which is not typically found in pristine or corona-treated PP film. Furthermore, a peak at 1187 cm^{-1} corresponding to the Si−O−C bending band suggests the formation of a covalent bond between the hydroxyl groups on the corona-treated PP and silica. The most significant peaks at 1357 and 1457 cm^{-1} belong to C−H rocking in methyl and C−H scissoring of the PP, respectively. Additional peaks are at 723 (C−C rocking), 803 (C−C stretching), 841 (C−H rocking), 937 (C−H rocking in methyl), 983 (C−H rocking in methyl), and 1157 cm^{-1} (C−O stretching).

FTIR was also used to study the surfaces of other coatings, and new peaks were observed in addition to those previously identified. The peaks at 698, 714, and 748 cm^{-1} correspond to the C−H out of plane bending band in the aromatic ring, while the peak at 1586 cm^{-1} corresponds to the C═C stretching band in the aromatic ring. These peaks are present in poly(TPPPETS) and SiO_2/poly(TPPPETS) coatings, which contain more aromatic rings compared to those in the SiO_2/poly(TOPPETS) coating. A peak corresponding to $C-P^+$ was found at 1510 cm^{-1}, indicating the presence of phosphonium at the surfaces of the coatings. However, this peak is much smaller for the SiO_2/poly(TOPPETS) coating due to its less uniform structure (Figure 7).

3.1.4. Coating Thickness and Uniformity. The thicknesses and uniformity of the coatings were studied by the FIB,

https://doi.org/10.1021/acsomega.3c04908
ACS Omega 2023, 8, 39354−39365

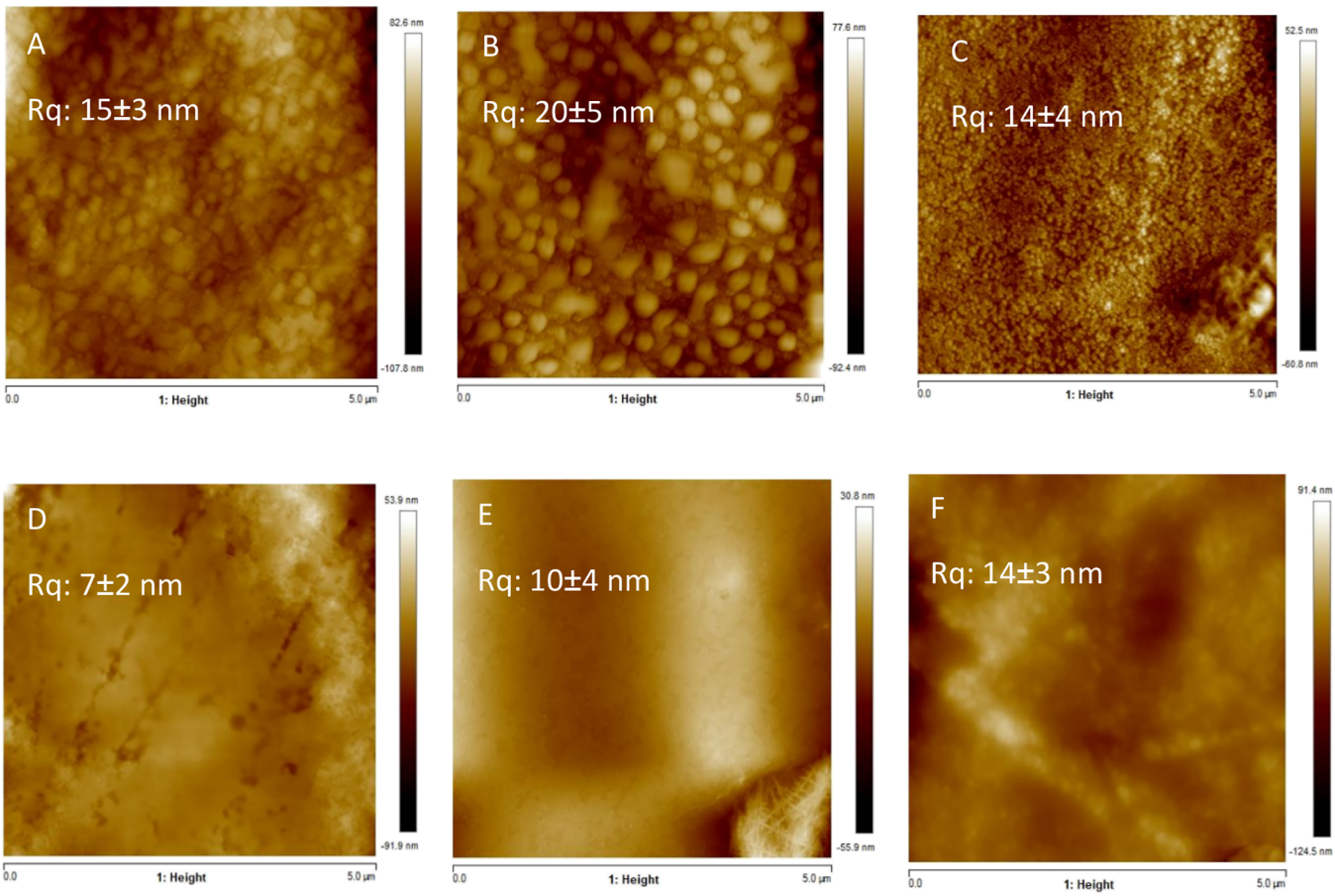

Figure 9. Surface morphology and roughness of the coatings/films. (A) PP, (B) corona-treated PP, (C) SiO_2, (D) poly(TPPPETS), (E) SiO_2/poly(TPPPETS), and (F) SiO_2/poly(TOPPETS).

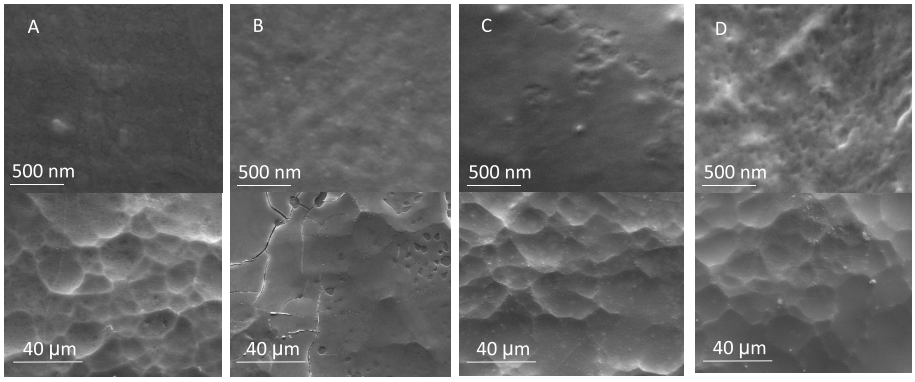

Figure 10. ESEM images in small and large scales for the coatings. (A) SiO_2, (B) poly(TPPPETS), (C)SiO_2/poly(TPPPETS), and (D) SiO_2/poly(TOPPETS).

Table 2. % Phosphorus as Measured by EDX

coatings	% phosphorus
SiO_2	0.0
poly(TPPPETS)	4.2
SiO_2/poly(TPPPETS)	3.9
SiO_2/poly(TOPPETS)	3.1

providing valuable information on coating characteristics. Although all coatings were made with the same no. 1 bar, the thicknesses are different. The SiO_2 and SiO_2/poly(TOPPETS) coatings are made from NPs (Figures 8A,D) while poly(TPPPETS) and SiO_2/poly(TPPPETS) are made from a uniform layer or made from NPs (Figures 8B,C). However, the NPs in the poly(TPPPETS) and SiO_2/poly(TPPPETS) coatings are very dense, the particulate nature of these coatings is negligible, and they are more uniform and smoother from the SiO_2 and SiO_2/poly(TOPPETS) coatings, which are made from NPs. Different NP sizes used in the polymerization process resulted in varying thicknesses of the coatings. Recent studies show that more bacteria can adhere to coating when the thickness of the coating decreases.[42−44] In other words, the biological activity of the coatings increases when the thickness increases, and

https://doi.org/10.1021/acsomega.3c04908
ACS Omega 2023, 8, 39354−39365

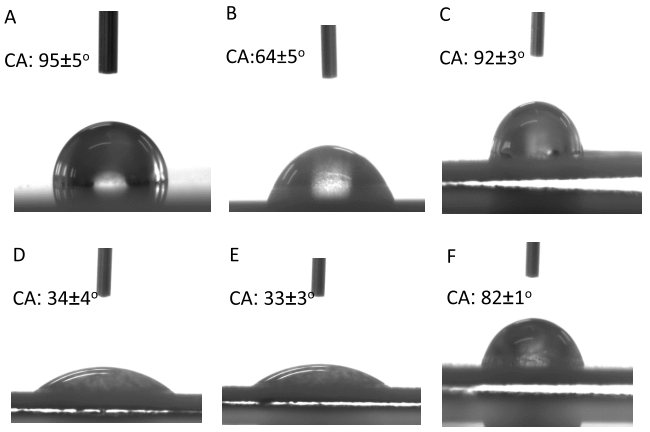

Figure 11. Water contact angles of the coatings/films. (A) PP, (B) corona-treated PP, (C) SiO_2, (D) poly(TPPPETS), (E) SiO_2/poly(TPPPETS), and (F) SiO_2/poly(TOPPETS).

Table 3. CA Values for Silane-Phosphonium Coatings after 10 Applications of the Tape Test[a]

coating	CA before tape test (deg)	CA after 10 tape tests (deg)
poly(TPPPETS)	34 ± 4	38 ± 2
SiO_2/poly(TPPPETS)	33 ± 3	34 ± 3
SiO_2/poly(TOPPETS)	82 ± 1	84 ± 3

[a]The change in the CA of each coating is negligible, which shows that the coatings are stable.

thicker coatings may be more efficient for medical and agricultural applications. However, additional parameters also influence the biological activity of the coatings, including the uniformity and roughness of the coatings. While the poly(TPPPETS) and SiO_2/poly(TPPPETS) coatings exhibited uniformity, the SiO_2 and SiO_2/poly(TOPPETS) coatings were less uniform. The particulate nature of the coatings made from NPs was negligible in the coatings, where the NPs were dense, resulting in a more uniform and smoother surface.

As mentioned above, the poly(TOPPETS) coating was not uniform. This is due to the less uniform dispersion for poly(TOPPETS) coating, resulting in unequal amounts of phosphonium at different points on the surface. However, the SiO_2/poly(TOPPETS) coating is more uniform due to the presence of SiO_2 core NPs, which aid in binding the silane-phosphonium monomer to the corona-treated PP surface. The SiO_2 coating, conversely, is less uniform than the coatings containing TPPPETS, highlighting the importance of the phosphonium moiety for achieving a uniform coating.

Table 4. ToBRFV Bioassay of Infected Tobacco Seedling Leaves

coating/film type	seedling no.	LLs	coating/film type	seedling no.	LLs
positive control	1	>100	SiO_2	12	43
positive control	2	>100	poly(TPPPETS)	13	0
positive control	3	67	poly(TPPPETS)	14	3
PP	4	20	poly(TPPPETS)	15	1
PP	5	51	SiO_2/poly(TPPPETS)	16	0
PP	6	48	SiO_2/poly(TPPPETS)	17	3
corona-treated PP	7	16	SiO_2/poly(TPPPETS)	18	2
corona-treated PP	8	46	SiO_2/poly(TOPPETS)	19	0
corona-treated PP	9	30	SiO_2/poly(TOPPETS)	20	6
SiO_2	10	>100	SiO_2/poly(TOPPETS)	21	1
SiO_2	11	50			

3.1.5. Morphology and Roughness of the Films. Surface morphology and roughness of the different films were analyzed using AFM and the results show that the corona-treated PP has the highest roughness, which was expected. The pristine PP used in this study was somewhat rough, which resulted in a relatively high roughness. The uniform poly(TPPPETS) and SiO_2/poly(TPPPETS) coatings were found to be less rough which is in line with FIB measurements that showed uniform and smooth coatings for poly(TPPPETS) and SiO_2/poly(TPPPETS) films (Figure 9).

3.1.6. Uniformity and Morphology of the Coatings by ESEM. As described above (Section 2.3.6), ESEM can provide additional information about the surfaces of the coatings.

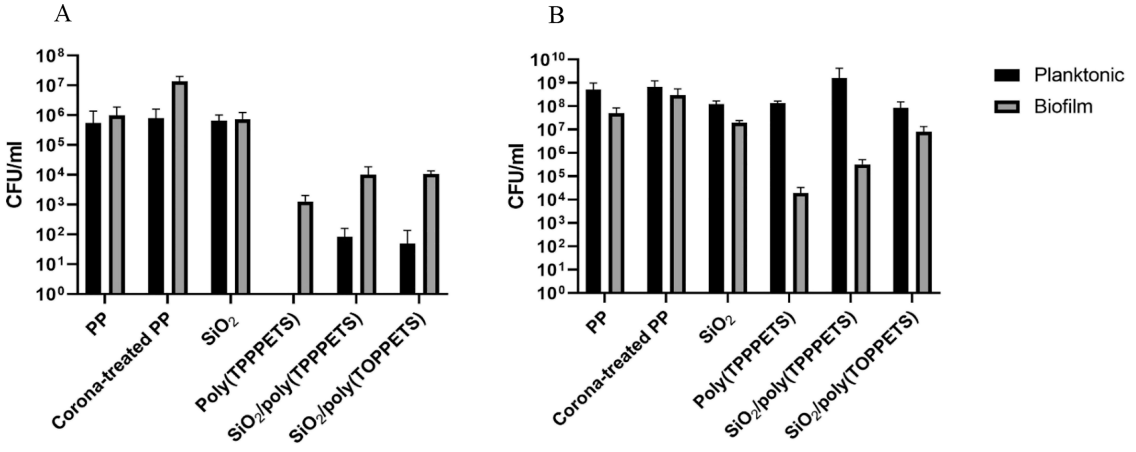

Figure 12. Antibiofilm and antibacterial activities of PP, corona-treated PP, and different coatings against (A) *S. aureus*and (B) *E. coli*. The graph is the average of three independent experiments with two internal repeats. Error bars represent the standard deviations.

https://doi.org/10.1021/acsomega.3c04908
ACS Omega 2023, 8, 39354−39365

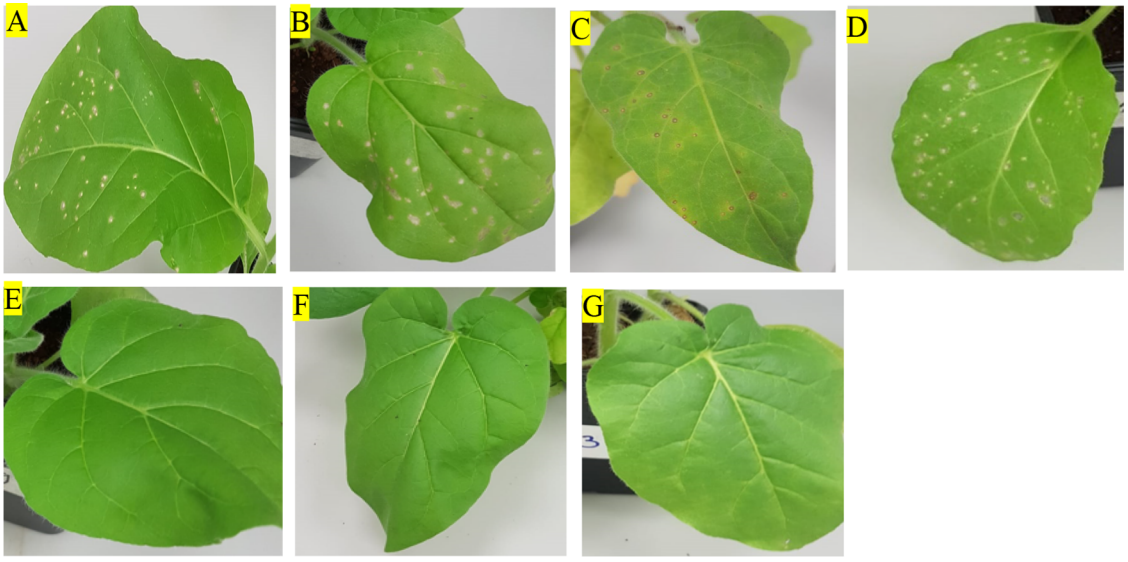

Figure 13. Biological assay of ToBRFV on *Nicotiana tabacum*plants of the different coatings/films. (A) Positive control, (B) corona-treated PP, (C)PP, (D) SiO_2, (E) Poly(TPPPETS), (F) SiO_2/poly(TPPPETS), (G) SiO_2/poly(TOPPETS). Photos were taken by Matan Nissim (author).

Table 5. ELISA Test Results of ToBRFV in Infected Tomato Seedling Leaves

coating/film type	seedling no.	ToBRFV ELISA results	coating/film type	seedling no.	ToBRFV ELISA results
positive control	1	+	SiO_2	12	+
positive control	2	+	poly(TPPPETS)	13	−
positive control	3	−	poly(TPPPETS)	14	−
PP	4	+	poly(TPPPETS)	15	−
PP	5	−	SiO_2/poly(TPPPETS)	16	−
PP	6	−	SiO_2/poly(TPPPETS)	17	−
corona-treated PP	7	+	SiO_2/poly(TPPPETS)	18	−
corona-treated PP	8	+	SiO_2/poly(TOPPETS)	19	−
corona-treated PP	9	−	SiO_2/poly(TOPPETS)	20	−
SiO_2	10	+	SiO_2/poly(TOPPETS)	21	+
SiO_2	11	+			

Figure 10 presents the surfaces of the different coatings on small and large scales. The ESEM results show that the coatings are uniform, particularly for poly(TPPPETS) and SiO_2/poly(TPPPETS) coatings, and support the results obtained from FIB and AFM measurements. In addition, EDX measurements (Table 2) show that phosphorus (phosphonium) existed on the surfaces of the poly-(TPPPETS), SiO_2/poly(TPPPETS), and SiO_2/poly-(TOPPETS) coatings and not existed on the surface of the SiO_2 coating.

3.1.7. Wettability of the Films. Water CA can provide insights into the polar nature of a surface. Our measurements revealed significant differences between the surfaces of the films, depending on their type. As expected, the contact angle of the untreated PP film was high, while the corona-treated PP film exhibited a much smaller contact angle. The poly-(TPPPETS) and SiO_2/poly(TPPPETS) coatings were uniform and displayed a lower contact angle, even compared to the corona-treated PP film. However, the SiO_2/poly(TOPPETS) coating exhibited a larger contact angle due to the free movement of the hydrophobic octyl groups, which could cover the phosphonium and increase the contact angle. Furthermore, this coating was less uniform, resulting in a larger contact angle. Therefore, this method may not be sensitive to this coating, as the contact angle is too large. Nevertheless, it can be a useful tool for determining the presence of polar and charged groups (such as phosphonium) on the surface of some films (such as PP) in coatings (such as poly(TPPPETS) and SiO_2/poly(TPPPETS)) (Figure 11).

3.1.8. Durability Test. As described in the methods (Section 2.3.8), CA measurements demonstrate the stability of the coatings. In addition, the coatings were tested after four months, which also demonstrates the stability of the coatings. Table 3 presents the CA before and after the tape test.

3.2. Biological Activities. *3.2.1. Antibiofilm activity.* Antibiofilm activity was tested against *S. aureus*and *E. coli*. For *S. aureus*, our results show high antibiofilm activity for all tested coatings, compared to the relevant control (PP, corona-treated PP, and SiO_2 coating), observed by a 4−5 log reduction in bacterial load on the surface (Figure 12A). Furthermore, a decrease in bacterial count in the surrounding media (planktonic bacteria) compared with the controls was observed, which correlated with the reduction in biofilm biomass. This significant antibacterial activity for all the tested coatings against *S. aureus*(a 4−5 log-reduction in planktonic bacteria) may explain the reduction in biofilm biomass, as there were less bacteria in the surrounding liquid free to attach to the surface and propagate.

A significant antibiofilm activity was found for poly-(TPPPETS) and SiO_2/poly(TPPPETS) against *E. coli*, exhibited by a 4-log and a 1-log reduction in biofilm biomass, respectively. However, no antibiofilm activity was found for

https://doi.org/10.1021/acsomega.3c04908
ACS Omega 2023, 8, 39354−39365

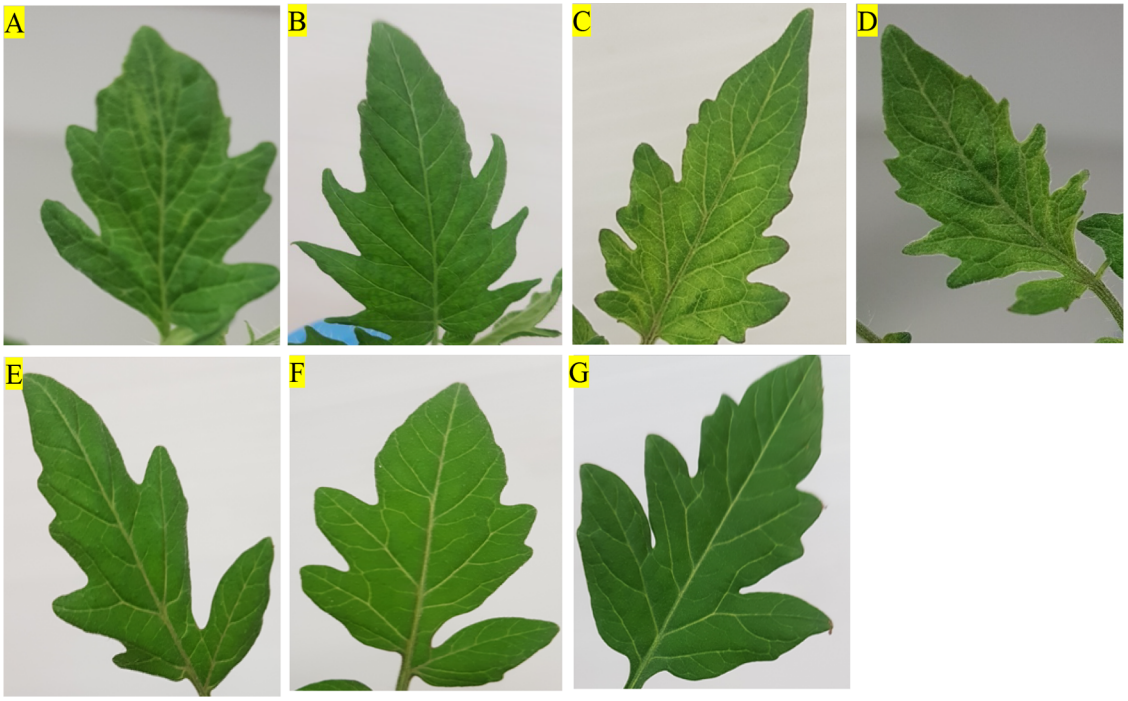

Figure 14. Biological assay of ToBRFV on tomato plants of the different coatings/films. (A) Positive control, (B) corona-treated PP, (C) PP, (D) SiO_2, (E) poly(TPPPETS), (F) SiO_2/poly(TPPPETS), (G) SiO_2/poly(TOPPETS). Photos were taken by Nissim (author).

SiO_2/poly(TOPPETS). There was also no observed antibacterial activity against planktonic *E. coli*by any of the coatings.

Our results show high antibacterial activity against *S. aureus*and a lack of activity against *E. coli*. The mechanism of action of phosphonium salts includes cytoplasmic and/or outer membrane abruption, depending on the gram-group. Cationic disinfectants, such as phosphonium salts, are known to be more effective against Gram-positive bacteria than Gram-negative, in which the outer membrane acts as a second barrier, corresponding with our results.[17,45] The reduced *E. coli*biofilm formation on poly(TPPPETS) and SiO_2/poly(TPPPETS) surfaces may be attributed to the coating's smoothness, as was found by FIB, AFM, and SEM (Figures 8−10). High surface roughness promotes biofilm formation due to high surface area and the physical protection it provides, and vice versa.[46−51] Roughness, in combination with the less uniform pattern of the coating, as was found by FIB, AFM, and SEM (Figures 8−10), may explain the SiO_2/poly(TOPPETS) coating's lack of antibiofilm effect. Nonetheless, the significant antibiofilm activity of the poly(TPPPETS) and SiO_2/poly-(TPPPETS) coatings against *E. coli*, even when having no effect on planktonic bacteria, emphasizes their importance as antibiofilm materials.

3.2.2. Antiviral Activity Against ToBRFV in Tobacco and Tomato Seedlings. The number of LLs can indicate the level of active viral particles that have infected the tobacco plant, making it a useful indicator for testing the antiviral activity of the phosphonium-coated polymers.[13] The number of LLs was counted, and the small number of lesions indicates significant antiviral activity of the substrate. After exposure to the virus pretreated with poly(TPPPETS), SiO_2/poly(TPPPETS), and SiO_2/poly(TOPPETS) coatings, there were none or a few LLs in the seedlings. These results testify to the antiviral efficacy of these coatings. In contrast, dozens of LLs were counted for each control (positive control, PP, corona-treated PP, and the SiO_2 coating), showing that there is no antiviral activity for these films/coatings. Hence, to protect seedlings from the virus, applying these coatings on doors, walls of greenhouses, agricultural devices, and desks can reduce the spreading of the virus. The virus particles, which find in the space, will become inactive ("dead") upon contact with these coated surfaces. In this way, the virus spreads, and the amount of virus particles can be reduced. As a result, more seedlings will be protected. Table 4 summarizes the results of the experiments, and Figure 13 presents seedlings with/without LLs.

ELISAs for tomato seedlings show the same trend for tomato seedlings. Eight of the 12 seedlings that were treated with controls (positive control, pp, corona-treated pp, and SiO_2 coating) were infected when just one from the nine seedlings that were treated with the phosphonium coatings (poly(TPPPETS), SiO_2/poly(TPPPETS), and SiO_2/poly-(TOPPETS)) was infected. These results match with the results for tobacco seedlings and show significant antiviral activity of the phosphonium coatings. Table 5 summarizes the results of the experiments, and Figure 14 presents seedlings.

4. SUMMARY AND CONCLUSIONS

The present study discussed the synthesis and characterization of silane-phosphonium coatings onto polymeric films with potential applications in medical, agricultural, and industrial fields. We successfully synthesized silane-phosphonium monomers and confirmed their synthesis through ^{31}P NMR and MS analysis. These monomers formed the basis for creating phosphonium coatings onto PP films using two different preparation methods. In the first method, a modified Stöber polymerization was applied to the silane-phosphonium monomer, and the coating was done immediately. In the second method, TEOS Stöber polymerization was done and after 30 min, the silane-phosphonium was added to the

https://doi.org/10.1021/acsomega.3c04908
ACS Omega 2023, 8, 39354−39365

dispersion. Our findings demonstrate that the choice of the phosphonium reagent is crucial for obtaining uniform coatings. For instance, the use of TEOS was necessary to achieve a uniform SiO_2/poly(TOPPETS) coating, compared to the poly(TOPPETS) coating was found to be nonuniform and ineffective without this reagent. We used FTIR to study the chemical composition of the various films' surfaces, and each film had a unique spectrum that reflected the relevant treatment used for its preparation. Moreover, we used AFM to investigate the roughness and morphology of the coatings. Our results revealed that corona-treated PP had the highest roughness due to the polar functional groups formed on its surface. Conversely, the coatings containing TPPPETS were found to be uniform and smooth, resulting in a lower roughness. These findings suggest that the presence of TPPPETS can lead to a more even distribution of the coating material on the polymeric film. The study investigated the antibiofilm and antiviral activity of phosphonium coatings synthesized by using silane-phosphonium monomers. The results for poly(TPPPETS) and SiO_2/poly(TPPPETS) showed significant antibiofilm activity against *S. aureus*and *E. coli*and promising antiviral activity against ToBRFV. The SiO_2/poly(TOPPETS) showed antibiofilm activity only against *S. aureus*. These findings hold promise for further research on various coatings and biological targets with the potential for the development of uniform coatings that can be fine-tuned for medical, agricultural, and industrial applications. Overall, the study demonstrates the potential of silane-phosphonium coatings as antibiofilm and antiviral surfaces.

AUTHOR INFORMATION

Corresponding Author

Shlomo Margel − *The Institute of Nanotechnology and Advanced Materials, Department of Chemistry, Bar-Ilan University, Ramat-Gan 5290002, Israel;* orcid.org/0000-0001-6524-8179; Email: Shlomo.Margel@biu.ac.il

Authors

Matan Nissim − *The Institute of Nanotechnology and Advanced Materials, Department of Chemistry, Bar-Ilan University, Ramat-Gan 5290002, Israel*

Taly Iline-Vul − *The Institute of Nanotechnology and Advanced Materials, Department of Chemistry, Bar-Ilan University, Ramat-Gan 5290002, Israel*

Sivan Shoshani − *The Institute of Nanotechnology and Advanced Materials, Faculty of life science, Bar-Ilan University, Ramat-Gan 5290002, Israel*

Gila Jacobi − *The Institute of Nanotechnology and Advanced Materials, Faculty of life science, Bar-Ilan University, Ramat-Gan 5290002, Israel;* orcid.org/0000-0001-5709-7219

Eyal Malka − *The Institute of Nanotechnology and Advanced Materials, Department of Chemistry, Bar-Ilan University, Ramat-Gan 5290002, Israel*

Aviv Dombrovsky − *Plant Pathology Department, Agricultural Research Organization-Volcani Institute, Rishon LeZion 7505101, Israel*

Ehud Banin − *The Institute of Nanotechnology and Advanced Materials, Faculty of life science, Bar-Ilan University, Ramat-Gan 5290002, Israel;* orcid.org/0000-0003-2974-5877

Complete contact information is available at: https://pubs.acs.org/10.1021/acsomega.3c04908

Author Contributions

M.N. did the methodology, conceptualization, and writing of the original draft. T.I.-V. performed the validation and writing—reviewing and editing. S.S. did the investigation and writing of the original draft. G.J. and E.M. did the methodology and validation. A.D. is the project manager and performed writing—reviewing and editing. E.B. supervised and performed writing—reviewing and editing. S.M. did the supervision and writing—reviewing and editing.

Notes

The authors declare no competing financial interest.

ACKNOWLEDGMENTS

The authors thank Prof. Edward Korshin for assistance with the synthesis and for helpful suggestions and Dr. Yuval Elias for editing the manuscript.

REFERENCES

(1) Balloux, F.; van Dorp, L. Q&A: What are pathogens, and what have they done to and for us? *BMC Biol.* **2017**, *15*, 91.

(2) Elias, S.; Banin, E. Multi-species Biofilms: Living with Friendly Neighbors. *Fed. Eur. Microbiol. Soc.* **2012**, *36*, 990−1004.

(3) Banin, E.; Brady, K. M.; Greenberg, E. P. Chelator-induced Dispersal and Killing of *Psedomonas aeruginosa* Cells in a Biofilm. *Appl. Environ. Microbiol.* **2006**, *72*, 2064−2069.

(4) Steinmetz, H. P.; Rudnick-Glick, S.; Natan, M.; Banin, E.; Margel, S. Graft Polymerization of Styryl Bisphosphonate Monomer onto Polypropylene Films for Inhibition of Biofilm Formation. *Colloids. Surf. B* **2016**, *147*, 300−306.

(5) Naik, K.; Kowshik, M. Anti-quorum Sensing Activity of AgCl-TiO_2 Nanoparticles with Potential Use as Active Food Packaging Material. *J. Appl. Microbiol.* **2014**, *117*, 972−983.

(6) Perez, E.; Williams, M.; Jacob, J. T.; Reyes, M. D.; Chernetsky Tejedor, S.; Steinberg, J. P.; Rowe, L.; Ganakammal, S. R.; Changayil, S.; Weil, M. R.; Donlan, R. M.; Patel, R. Microbial Biofilms on Needleless Connectors for Central Venous Catheters: Comparison of Standard and Silver-coated Devices Collected from Patients in an Acute Care Hospital. *J. Clin. Microbiol.* **2014**, *52*, 823−831.

(7) Chauhan, A.; Lebeaux, D.; Ghigo, J. M.; Beloin, C. Full and Broad-spectrum *in vivo* Eradication of Catheter-Associated Biofilms using Gentamicin-EDTA Antibiotic Lock Therapy. *Antimicrob. Agents Chemother.* **2012**, *56*, 6310−6318.

(8) Rose, R. K. The role of calcium in oral streptococcal aggregation and the implications for biofilm formation and retention. *Biochim. Biophys. Acta* **2000**, *1475* (1), 76−82.

(9) Shukla, S. K.; Rao, T. S. Effect of Calcium on *Staphylococcus aureus* Biofilm Architecture: a Confocal Laser Scanning Microscopic Study. *Colloids Surf., B* **2013**, *103*, 448−454.

(10) Prestinaci, F.; Pezzotti, P.; Pantosti, A. Antimicrobial Resistance: a Global Multifaceted Phenomenon. *Pathog. Glob. Health.* **2015**, *109*, 309−318.

(11) Oladokun, J. O.; Halabi, M. H.; Barua, P.; Nath, P. D. Tomato brown rugose fruit disease: current distribution, knowledge and future prospects. *Plant Pathol.* **2019**, *68*, 1579−1586.

(12) Malka, E.; Dombrovsky, A.; Margel, S. Preparation and Characterization of a Novel PVA/PVP Hydrogel containing Entrapped Hydrogen Peroxide for Agricultural Applications. *ACS. J. Agric. Sci.* **2022**, *2*, 430−436.

(13) Steinman, N. Y.; Hu, T.; Dombrovsky, A.; Reches, M.; Domb, A. J. Antiviral Polymers Based on N-Halamine Polyurea. *ACS Biomacromolecules.* **2021**, *22* (10), 4357−4364.

(14) Luria, N.; Smith, E.; Reingold, V.; Bekelman, I.; Lapidot, M.; Levin, I.; Elad, N.; Tam, Y.; Sela, N.; Abu-Ras, A.; Ezra, N.; Haberman, A.; Yitzhak, L.; Lachman, O.; Dombrovsky, A.; Melcher, U. A new Israeli Tobamovirus isolate infects tomato plants harboring Tm-22 Resistance Genes. *PLOS One* **2017**, *12*, No. e0170429.

(15) Eldan, O.; Ofir, A.; Luria, N.; Klap, C.; Lachman, O.; Bakelman, E.; Belausov, E.; Smith, E.; Dombrovsky, A. Pepper Plants Harboring *L* Resistance Alleles Showed Tolerance toward Manifestations of Tomato Brown Rugose Fruit Virus Disease. *Plants.* **2022**, *11*, 2378.
(16) Salem, N.; Mansour, A.; Ciuffo, M.; Falk, B. W.; Turina, M. A new tobamovirus infecting tomato crops in Jordan. *Arch. Virol.* **2016**, *161* (2), 503−506.
(17) Xue, Y.; Xiao, H.; Zhang, Y. Antimicrobial Polymeric Materials with Quaternary Ammonium and Phosphonium Salts. *Int. J. Sci.* **2015**, *16*, 3626−3655.
(18) Kanazawa, A.; Ikeda, T.; Endo, T. Synthesis and antimicrobial activity of dimethyl- and trimethyl- substituted phosphonium salts with alkyl chains of various lengths. *Antimicrob. Agents Chemother.* **1994**, *38* (5), 945−952.
(19) Kanazawa, A.; Ikeda, T.; Endo, T. Novel polycationic biocides: synthesis and antibacterial activity of polymeric phosphonium salts. *J. Polym. Sci., Part A: Polym. Chem.* **1993**, *31*, 335−343.
(20) Kanazawa, A.; Ikeda, T.; Endo, T. Polymeric phosphonium salts as a novel class of cationic biocides. II. Effects of counter anion and molecular weight on antibacterial activity of polymeric phosphonium salts. *J. Polym. Sci.* **1993**, *31*, 1441−1447.
(21) Kanazawa, A.; Ikeda, T.; Endo, T. Polymeric phosphonium salts as a novel class of cationic biocides. IV. Synthesis and antibacterial activity of polymers with phosphonium salts in the main chain. *J. Polym. Sci., Part A: Polym. Chem.* **1993**, *31*, 3031−3038.
(22) Kanazawa, A.; Ikeda, T.; Endo, T. Polymeric phosphonium salts as a novel class of cationic biocides. VII. Synthesis and antibacterial activity of polymeric phosphonium salts and their model compounds containing long alkyl chains. *J.Appl.Polym.Sci.* **1994**, *53*, 1237−1244.
(23) Sousa Junior, R. R. d.; Gouveia, J. R.; Nacas, A. M.; Tavares, L. B.; Ito, N. M.; Moura, E. N. d.; Gaia, F. A.; Pereira, R. F.; Santos, D. J. d. Improvement of Polypropylene Adhesion by Kraft Lignin Incorporation. *Mater. Res.* **2019**, *22*, 2.
(24) Ding, L.; Zhang, X.; Wang, Y. Study on the Behavior of BOPP film Treated by Corona Discharge. *Coat.* **2020**, *10*, 1995.
(25) Sun, C.; Zhang, D.; Wadsworth, L. C. Corona treatment of polyolefin films-a review. *Adv.Polym.Technol.* **1999**, *18* (2), 171−180.
(26) Linder, M.; Rodler, N.; Jesdinszki, M.; Schmidt, M.; Sängerlaub, S. Surface energy of corona treated PP, PE and PET films, its alteration as function of storage time and the effect of various corona dosages on their bond strength after lamination. *J.Appl.Polym.Sci.* **2018**, *135*, 11.
(27) Żenkiewicz, M. Investigation on the oxidation of surface layers of polyolefins treated with corona discharge. *J. Adhes. Sci. Technol.* **2001**, *15* (1), 63−70.
(28) Strobel, M.; Lyons, C. S.; Strobel, J. M.; Kapaun, R. S. Analysis of air-corona-treated polypropylene and poly(ethylene terephthalate) films by contact-angle measurements and X-ray photoelectron spectroscopy. *J. Adhes. Sci. Technol.* **1992**, *6* (4), 429−443.
(29) Sapieha, S.; Cerny, J.; Klemberg-Sapieha, J.; Martinu, L. Corona versus low pressure plasma treatment: effect on surface properties and adhesion of polymers. *J. Adhes.* **1993**, *42*, 91−102.
(30) Pascual, M.; Sanchis, R.; Sánchez, L.; García, D.; Balart, R. Surface modification of low-density polyethylene (LDPE) film using corona discharge plasma for technological applications. *J. Adhes. Sci. Technol.* **2008**, *22* (13), 1425−1442.
(31) Owens, D. K. The mechanism of corona and ultraviolet light-induced self-adhesion of poly (ethylene terephthalate) film. *J. Appl. Polym. Sci.* **1975**, *19* (12), 3315−3326.
(32) Lynch, J. B.; Spence, P. D.; Baker, D. E.; Postlethwaite, T. A. Atmospheric pressure plasma treatment of polyethylene via a pulse dielectric barrier discharge: Comparison using various gas compositions versus corona discharge in air. *J. Appl. Polym. Sci.* **1999**, *71* (2), 319−331.
(33) Wolf, R.; Sparavigna, A. C. Role of plasma surface treatments on wetting and adhesion. *Eng.* **2010**, *2* (6), 397−402.
(34) Wang, J.; Liang, M.; Fang, Y.; Qiu, T.; Zhang, J.; Zhi, L. Rod-coating: towards large-area fabrication of uniform reduced graphene oxide films for flexible touch screens. *Adv. Mater.* **2012**, *24* (21), 2874−2878.
(35) Sason, E.; Kolitz-Domb, M.; Chill, J. H.; Margel, S. Engineering of durable antifog thin coatings on plastic films by UV-curing of proteinoid prepolymers with PEG-diacrylate monomers. *ACS Omega.* **2019**, *4* (5), 9352−9360.
(36) Malka, E.; Caspi, A.; Cohen, R.; Margel, S. Fabrication and characterization of hydrogen peroxide and thymol loaded PVA/PVP hydrogel coatings as a novel anti-mold surface for hay protection. *Polymers.* **2022**, *14*, 28.
(37) Bretler, S.; Kanovski, N.; Iline-Vul, T.; Cohen, S.; Margel, S. In-situ thin coating of silica micro/nano-particles on polymeric films and their anti-fogging application. *Colloids Surf., A* **2020**, *607*, No. 125444.
(38) Iline-Vul, T.; Bretler, S.; Cohen, S.; Perelshtein, I.; Perkas, N.; Gedanken, A.; Margel, S. Engineering of superhydrophobic silica microparticles and thin coatings on polymeric films by ultrasound irradiation. *Mater. Today Chem.* **2021**, *21*, No. 100520.
(39) Iline-Vul, T.; Kanovsky, N.; Yom-Tov, D.; Nadav-Tsubery, M.; Margel, S. Design of silane-based UV-absorbing thin coatings on polyethylene films. *Colloids Surf., A* **2022**, *684*, No. 129164.
(40) Kanovsky, N.; Cohen, S.; Margel, S. In-situ design, characterization and use of durable superhydrophobic thin coatings applied on polymeric films. *Mater. Res. Bull.* **2022**, *146*, No. 111598.
(41) Koenig, R. Indirect ELISA methods for the broad specificity detection of plant viruses. *J.Gen.Virol.* **1981**, *55*, 53−62.
(42) Kolewe, K. W.; Zhu, J.; Mako, N. R.; Nonnenmann, S. S.; Schifmann, J. D. Bacterial adhesion is affected by the thickness and stiffness of Poly(Ethylene glycol) hydrogels. *ACS. Appl. Mater. Interfaces.* **2018**, *10* (3), 2275−2281.
(43) Yadav, V.; Jaimes-Lizcano, Y. A.; Dewangen, N. K.; Park, N.; Li, T. H.; Robertson, M. L.; Conard, J. C. Tunning bacterial attachment and detachment via the thickness and dispersity of a PH-responsive polymer brush. *ACS. Appl. Matter. Interfaces.* **2017**, *9* (51), 44900−44910.
(44) Keskin, O.; Mergel, O.; Van der Mei, H. C.; Busscher, H. J.; Van Rijn, P. Inhibiting bacterial adhesion by mechanically modulated microgel coating. *ACS Biomacromol.* **2019**, *20*, 243−253.
(45) McDonnell, G.; Russell, A. D. Antiseptics and disinfectants: Activity, action and resistance. *Clin. Microbiol. Rev.* **1999**, *12* (1), 147−179.
(46) Zheng, S.; Bawazir, M.; Dhall, A.; Kim, H. E.; He, L.; Heo, J.; Hwang, G. Implication of Surface Properties, Bacterial Motility, and Hydrodynamic conditions on Bacterial Surface Sensing and Their Initial Adhesion. *Front. Bioeng. Biotechnol.* **2021**, *9*, No. 643722.
(47) Xing, R.; Lyngstadaas, S. P.; Ellingsen, J. E.; Taxt-Lamolle, S.; Haugen, H. J. The influence of surface nanoroughness, texture and chemistry of TiZr implant abutment on oral biofilm accumulation. *Clin. Oral Implants Res.* **2015**, *26* (6), 649−656.
(48) Yu, P.; Wang, C.; Zhou, J.; Jiang, L.; Xue, J.; Li, W. Influence of surface properties on Adhesion forces and Attachment of streptococcus mutans to Zirconia In vitro. *Biomed Res. Int.* **2016**, 8901253.
(49) Yao, W. L.; Lin, J. C. Y.; Salamanca, E.; Pan, Y. H.; Tsai, P. Y.; Leu, S. J.; Yang, K. C.; Huang, H. M.; Huang, H. Y.; Chang, W. J. Cr: YSGG Laser performance improves Biological Response on Titanium Surfaces. *Materials* **2020**, *13* (3), 756.
(50) Yoda, I.; Koseki, H.; Tomita, M.; Shida, T.; Horiuchi, H.; Sakoda, H.; Oseki, M. Effect of surface roughness of biomaterials on staphylococcus epidermidis adhesion. *BMC Microbiol.* **2014**, *14*, 234.
(51) Bollen, C. M. L.; Papaioanno, W.; Van Eldre, J.; Schepers, E.; Quirynen, M.; Van Steenberghe, D. The influence of abutment surface roughness on plaque accumulation and Peri-implant mucositis. *Clin. Oral Implants Res.* **1996**, *7* (3), 201−211.

https://doi.org/10.1021/acsomega.3c04908
ACS Omega 2023, 8, 39354−39365